PDGF-induced migration of synthetic vascular smooth muscle cells through c-Src-activated L-type Ca^{2+} channels with full-length $Ca_V1.2$ C-terminus

Xiaoguang Guo[1, 2#], Toshihide Kashihara[1#], Tsutomu Nakada[1], Toshifumi Aoyama[2], Mitsuhiko Yamada[1*]

[1] Department of Molecular Pharmacology, Shinshu University School of Medicine, Matsumoto, Nagano, Japan; [2] Department of Metabolic Regulation, Institute on Aging and Adaptation, Shinshu University Graduate School of Medicine, Matsumoto, Nagano, Japan

*Corresponding author:
Mitsuhiko Yamada, M.D. Ph.D.
3-1-1 Asahi, Matsumoto, Nagano 390-8621 Japan
TEL: +81-263-37-2605
E-mail: myamada@shinshu-u.ac.jp

[#] These two authors equally contributed to this work.

ORCID: Mitsuhiko Yamada: 0000-0002-7515-3824

Abstract

In atherosclerosis, vascular smooth muscle cells (VSMC) migrate from the media toward the intima of the arteries in response to cytokines, such as platelet-derived growth factor (PDGF). However, molecular mechanism underlying the PDGF-induced migration of VSMCs remains unclear. The migration of rat aorta-derived synthetic VSMCs, A7r5, in response to PDGF was potently inhibited by a $Ca_V1.2$ channel inhibitor, nifedipine, and a Src family tyrosine kinase (SFK)/Abl inhibitor, bosutinib, in a less-than-additive manner. PDGF significantly increased $Ca_V1.2$ channel currents without altering $Ca_V1.2$ proteins expression levels in A7r5 cells. This reaction was inhibited by C-terminal Src kinase, a selective inhibitor of SFKs. In contractile VSMCs, the C-terminus of $Ca_V1.2$ is proteolytically cleaved into proximal and distal C-termini (PCT and DCT, respectively). Clipped DCT is noncovalently reassociated with PCT to autoinhibit the channel activity. Conversely, in synthetic A7r5 cells, full-length $Ca_V1.2$ ($Ca_V1.2FL$) is expressed much more abundantly than truncated $Ca_V1.2$. In a heterologous expression system, c-Src activated $Ca_V1.2$ channels composed of $Ca_V1.2FL$ but not truncated $Ca_V1.2$ ($Ca_V1.2\Delta1763$) or $Ca_V1.2\Delta1763$ plus clipped DCT. Further, c-Src enhanced the coupling efficiency between the voltage-sensing domain and activation gate of $Ca_V1.2FL$ channels by phosphorylating Tyr1709 and Tyr1758 in PCT. Compared with $Ca_V1.2\Delta1763$, c-Src could more efficiently bind to and phosphorylate $Ca_V1.2FL$ irrespective of the presence or absence of clipped DCT. Therefore, in atherosclerotic lesions, phenotypic switching of VSMCs may facilitate pro-migratory effects of PDGF on VSMCs by suppressing posttranslational $Ca_V1.2$ modifications.

Key Words

Vascular smooth muscle cells, Platelet-derived growth factor, $Ca_V1.2$ channels, c-Src

Acknowledgement

We are grateful to Dr. Tuck Wah Soong (National University of Singapore, Singapore, Singapore) for kindly providing cDNA encoding rat smooth muscle $Ca_V1.2$ (B8 clone), to Dr. Toshikazu Takeshita (Shinshu University, Japan) for kindly providing anti-c-Src antibody, and to Ms. Reiko Sakai for secretarial assistance. This study was supported by Grant-in-Aid for Scientific Research (C) (grant number 16K08546) to T.K. from the Ministry of Education, Culture, Sports, Science and Technology, Japan and a grant to M.Y. from Shinshu Public Utility Foundation for Promotion of Medical Sciences.

Introduction

Despite recent improvements in life style and advances in pharmacotherapy, atherosclerosis remains to be a cause of various cardiovascular diseases, such as ischemic heart diseases, which are the leading cause of death in developed nations. Therefore, it is necessary to further explore the pathophysiology of atherosclerosis.

In the presence of atherosclerotic risk factors, such as hypercholesterolemia, the initial lesions of atherosclerosis are formed as "fatty streaks," in which circulating monocytes and T lymphocytes invade the sub-endothelial intimal layer of the large and medium arteries [20]. Macrophages derived from these monocytes secrete various cytokines, such as platelet-derived growth factor (PDGF). These cytokines cause a phenotypical switching of vascular smooth muscle cells (VSMC) from "contractile" to "synthetic" types. Further, PDGF potently induces the migration of synthetic VSMCs from the media into the intima of the arteries [25]. Synthetic VSMCs in the intima proliferate and efficiently secrete extracellular matrix, pathologically narrowing the vascular lumen, thereby leading to cardiovascular complications.

PDGF is a homo- or heterodimer encoded by four genes, PDGF-A, PDGF-B, PDGF-C, and PDGF-D. It acts on cells by binding to homo- or heterodimers of two PDGF receptors (PDGFRs), PDGFR-α and PDGFR-β [6]. Stimulated PDGFRs activate many intracellular signaling proteins, such as c-src family kinases (SFK), phosphatidylinositol-3 kinase (PI3K), mitogen-activated protein kinases (MAPK), phospholipase C-γ, Rho family GTPases (RFG), etc. Among them, SFK, PI3K, MAPK, and RFG have been implicated to play a role in cell migration [11].

Intracellular Ca^{2+} also plays a crucial role in cell migration, [15, 31`]. In migrating cells, Ca_V1 Ca^{2+} channels evoke Ca^{2+} sparklets at their rear end, thereby increasing the intracellular Ca^{2+} concentration and causing actomyosin contraction to retract their trailing tail [18]. VSMCs express L-type $Ca_V1.2$ channels, which play a role in migration [4] [21]. However, it is not entirely clear how an array of PDGFR-

derived signals orchestrates with the activity of $Ca_V1.2$ channels during VSMC migration.

$Ca_V1.2$ is the main pore-forming subunit of $Ca_V1.2$ channels, with 24 transmembrane segments divided into four domains and cytoplasmic N- and C-termini [35]. Each domain contains six transmembrane segments (S1-6). The pseud-heterotetrameric channel pore comprising S5-6 derived from each domain is symmetrically surrounded by four voltage-sensing domains (VSDs) formed by S1-4 of each domain [3]. The internal part of S6 serves as an activation gate (AG) of the channel. VSDs open AG through an intracellular S4-5 linker in the same domain upon membrane depolarization. A total of 10 of the 53 known $Ca_V1.2$ exons undergo alternative splicing. Tang et al. have observed that the most prevalent splice variant of $Ca_V1.2$ in the rat aorta (designated B8) bears exons 1, 8, 21, 32, and 33 and lacks exon 9* [30]. Vascular isoforms of $Ca_V1.2$ form vascular $Ca_V1.2$ channels with ancillary subunits, such as β_2 or β_3 and $\alpha_2\delta_1$ subunits [29].

The C-terminus of $Ca_V1.2$ is proteolytically cleaved into proximal and distal C-termini (PCT and DCT, respectively) in muscle cells and neurons [5] [13]. These posttranslational modifications produce two distinct molecular sizes (i.e., ~240 and ~210 KDa) of $Ca_V1.2$ in contractile VSMCs [1, 2, 22, 23, 33]. Cleaved DCT is noncovalently reassociated with PCT, autoinhibiting the channel activity [2, 8, 14, 19, 32]. In cardiac myocytes, protein kinase A (PKA) and casein kinase (CK) 2 activate $Ca_V1.2$ channels by inhibiting the autoinhibitory effect of the cleaved and reassociated DCTs [9] [17]. However, the functional significance of posttranslational modification in terms of $Ca_V1.2$ channel activity regulation in VSMCs remains unknown.

In the present study, we demonstrated the PDGF-induced migration of synthetic VSMCs through the activation of L-type Ca^{2+} channels with full-length $Ca_V1.2$ C-terminus through c-Src.

Methods

Animals

All animals used in the present study received humane care in compliance with the Guide for the Care and Use of Laboratory Animals published by the US National Institutes of Health. All experimental procedures were performed in accordance with the Guidelines for Animal Experimentation of Shinshu University and approved by the Committee for Animal Experimentation (Approval number 260017). Male Sprague–Dawley rats (200–220 g) were anesthetized with 0.3 mg/kg medetomidine (Domitor, Nippon Zenyaku Kogyo Co., Fukushima, Japan), 4.0 mg/kg midazolam (Midazolam Sandoz, Novartis, Tokyo, Japan), and 5.0 mg/kg butorphanol (Vetorphale, Meiji Seika Pharma Co., Tokyo, Japan). All animals were procured from Japan SLC Inc. (Hamamatsu, Japan).

Isolation of tissues

Rats were anesthetized and euthanized by exsanguination. The hearts were immediately excised and immersed in ice-cold modified Tyrode solution containing (mM) 136.5 NaCl (Wako Pure Chemical Industries, Osaka, Japan), 5.4 KCl (Wako), 1.8 $CaCl_2$ (Wako), 0.53 $MgCl_2$ (Wako), 5.5 HEPES (Dojindo, Kumamoto, Japan), and 5.5 glucose (Wako) (pH 7.4 with NaOH). The aorta and cerebral arteries were carefully dissected from the thorax and brain, respectively, and rinsed with the modified Tyrode solution.

Cell cultures

A7r5 smooth muscle cells derived from the rat thoracic aorta (American Type Culture Collection, Manassas, VA, USA) and tsA201 human embryonic kidney cells (European Collection of Authenticated Cell, Salisbury, UK) were cultured in the high-glucose (4.5 g/l) and low-glucose (1 g/l) Dulbecco's modified Eagle's medium (DMEM) supplemented with 10% fetal bovine serum (FBS, Sigma-Aldrich Japan, Tokyo,

Japan), 100 units/ml penicillin (Thermo Fisher Scientific, Waltham, MA, USA), and 100 μg/ml streptomycin (Thermo), respectively, at 37°C and 5% CO_2.

Plasmid construction

cDNA encoding a rat smooth muscle $Ca_V1.2$ (B8 clone) was kindly provided by Dr. Tuck Wah Soong (National University of Singapore, Singapore, Singapore) [30]. $Ca_V1.2\Delta1763$ [$Ca_V1.2$ subunit lacking a distal C-terminus$_{1764–2140}$ (DCT)] was generated using PCR. For the plasmid construction of HA-tagged $Ca_V1.2$ and HA-$Ca_V1.2\Delta1763$, an HA-epitope was inserted into N-termini using a sense primer containing a sequence coding HA-epitope tag and *Bam*HI site. The PCR products were subcloned into a blunt-ended pBlueScript SK-vector and subcloned again into the *Bam*HI sites of $Ca_V1.2$ sequence and plasmid multi-cloning sites. To generate 3xFLAG-tagged $Ca_V1.2$ DCT, cDNA encoding amino acids 1764–2140 of $Ca_V1.2$ was PCR-amplified and subcloned into p3xFLAG-CMV-10 (Sigma-Aldrich). Other cDNA included in the rat or mouse heart cDNA library were isolated using RT-PCR and were subcloned into pcDNA3.1 or pCMV-Myc (Clontech Laboratories, Mountain View, CA, USA) as previously reported [17, 28]. Single or multi-amino acid substitution mutants of $Ca_V1.2$ with their tyrosine residues of the C-terminus substituted with phenylalanine residues (Fig. 5) were generated using the QuickChange Site-Directed Mutagenesis Kit (Stratagene, Agilent Technologies, Tokyo, Japan) according to manufacturer's instructions.

Wound healing assay

A7r5 cells in collagen-coated 24-well plates were wounded by dragging a sterile 200 μl pipette tip (Labcon, Petaluma, CA, USA) across 100% confluent monolayers to create cell-free area. Then, the cells were treated with deionized water (control) or PDGF-BB (10 ng/ml, Bachem, Torrance, CA, USA) in the presence or absence of pharmacological inhibitors in serum-free DMEM for 48 h. The cells were fixed

in 4% paraformaldehyde in phosphate buffered saline for 15 min and stained with Phalloidin–tetramethylrhodamine B isothiocyanate (1 μg/ml, Sigma-Aldrich) and Hoechst 33342 (0.5 μg/ml, Sigma-Aldrich). Fluorescence images were acquired and digitized using an inverted fluorescent microscope (Zeiss Axio Observer Z1, Carl Zeiss, Jena, Germany). The extent of wound healing was evaluated as the ratio of the number of pixels of a healed area to that of the original wound area using a contrast adjustment configuration in the ImageJ software (NIH, MD, USA).

Ca^{2+} imaging

A7r5 cells plated to ~50% confluency on collagen-coated glass bottom 35-mm dishes were cultured in serum-free DMEM for 48 h to induce growth arrest, and the cells were treated with deionized water (control) or 10 ng/ml PDGF-BB for 24 h. Then, the samples were incubated with 2 μM Fluo-4/AM (Dojindo) plus 0.01% Cremophore EL (Sigma-Aldrich) and 0.02% BSA (Sigma-Aldrich) in serum-free DMEM for 30 min at 37°C and 5% CO_2. Following the treatment with vehicle (0.01% DMSO) or pharmacological inhibitors for 30 min and perfusion with normal or 60 mM KCl Tyrode solution, fluorescence images were acquired and digitized with an LSM 7 LIVE laser-scanning microscope every 0.5 s (Carl Zeiss). To assess the time course of intracellular Ca^{2+} concentration ($[Ca^{2+}]_i$) change, the increment in fluorescence intensity normalized to baseline fluorescence intensity ($\Delta F/F_0$) was calculated.

Electrophysiology

A7r5 cells were grown to ~70% confluency in plastic dishes and transiently transfected with cDNA for enhanced green fluorescent protein (EGFP, 0.1 μg plasmid DNA/35-mm dish) plus mock or C-terminal Src kinase (CSK) cDNA (1.0 μg plasmid DNA/35-mm dish) with Lipofectamine 2000 (Thermo). The cultures were maintained in a serum-free condition for 48 h. Then, the transfected cells were treated with vehicle (deionized water) or 10 ng/ml PDGF-BB for 24 h. Finally, the cells were detached and re-

plated onto coverslips at a low density in serum-free DMEM for 2 h before measuring $Ca_V1.2$ channel currents.

TsA201 cells were grown to ~70% confluency in plastic dishes and transiently transfected with an equimolar ratio of cDNA encoding wild-type or mutant $Ca_V1.2\alpha_{1C}$, β_{2a}, and $\alpha_2\delta_1$ subunits (1.0, 0.7, and 0.8 μg of plasmid DNA/35-mm dish, respectively); a 10-fold lower concentration of cDNA for EGFP; and cDNA for other proteins with polyethylenimine (4 μg/ml, Polysciences, Inc., Warrington, PA). The cultures were maintained in a serum-free condition for 48 h. Then, the cells were detached and re-plated onto collagen-coated coverslips at a low density in serum-free DMEM for 24 h.

Ionic currents of $Ca_V1.2$ channels were recorded from EGFP-positive A7r5 cells in the whole-cell configuration of the patch-clamp method at 35–36°C with a patch-clamp amplifier (Axopatch 200B, Molecular Devices, Sunnyvale, CA, USA). A pipette solution contained (mM) 90 D-glutamate (Wako), 20 TEA-Cl (Tokyo Chemical Industry, Tokyo, Japan), 10 EGTA (Dojindo), 20 HEPES, 10 N-methyl-D(–)-glucamine (Wako), 2 $MgCl_2$, and 3 MgATP (Sigma-Aldrich) (pH 7.3 with CsOH). The extracellular bath solution contained (mM) 150 N-methyl-D(–)-glucamine, 10 $BaCl_2$ (Wako), 5.4 CsCl (Wako), 1.2 $MgCl_2$, 5 HEPES, and 5.5 glucose (pH 7.4 with HCl). $Ca_V1.2$ channel currents were measured as the current inhibited by Cd^{2+} (100 μM, Wako). The relationship between the current density and voltage of $Ca_V1.2$ channels was analyzed according to the standard voltage protocol. The peak of $Ca_V1.2$ channel Ba^{2+} current density (pA/pF) was calculated by dividing the peak channel current amplitude by the cell membrane capacitance and plotted against the membrane potentials. The liquid junction potential of +20 mV between these pipette and bath solutions was corrected in the membrane potentials indicated in the following descriptions.

The coupling efficiency between the VSD and AG of recombinant $Ca_V1.2$ channels was assessed in EGFP-positive tsA201 cells with the above pipette and bath solutions as follows: (1) first, the membrane potential was depolarized from the holding potential of −80 mV to potentials between +50 mV and +80 mV for 25 ms with a 2-mV increment and then repolarized to −70 mV for 10 ms every 5 s; (2) then, the gating

charge was measured by integrating the ON gating current at the apparent reversal potential of $Ca_V1.2$ currents (E_{rev}) for initial 2 ms; and (3) finally, the coupling efficiency was assessed by calculating the ratio of the tail Ba^{2+} current amplitude upon repolarization from E_{rev} to −70 mV to the ON gating charge at E_{rev} [17].

The relationship between the current density and voltage of recombinant $Ca_V1.2$ channels in tsA201 cells was analyzed according to the standard voltage protocol with the above pipette solution and the bath solution in which Ba^{2+} was substituted with 10 mM Ca^{2+}.

Steady-state activation curve of recombinant $Ca_V1.2$ channels was assessed by fitting the peak current density–voltage curve of $Ca_V1.2$ Ca^{2+} channel currents into the following equation (Table 1):

$$D_{\_peak} = G_{max} (1 / (1 + exp ((E_{0.5\_Act} - E_m) / k_{\_Act}))) (E_m - E_{rev}) \quad \text{(Eq. 1)}$$

$D_{\_peak}$, peak current density; G_{max}, maximum conductance density; $E_{0.5\_Act}$, half-maximum activation potential; E_m, membrane potential; and $k_{\_Act}$, slope factor of activation. From $E_{0.5\_Act}$ and $k_{\_Act}$, the activation curve of recombinant $Ca_V1.2$ channels was depicted using the Delta Graph software (Pantone Inc., NJ, USA).

The steady-state inactivation of recombinant $Ca_V1.2$ channels was assessed according to the standard double-pulse protocol, and the peak $Ca_V1.2$ channel Ca^{2+} current amplitude in P2 normalized to the maximum was plotted against P1 membrane potentials and fit into the following equation (Table 1):

$$f = f_0 + (1 - f_0) / (1 + exp ((E_m - E_{0.5\_Inact}) / k_{\_Inact})) \quad \text{(Eq. 2)}$$

f, availability; f_0, *an offset at depolarized potential;* $E_{0.5\_Inact}$, half-maximum inactivation potential; and $k_{\_Inact}$, slope factor of inactivation.

Immunoblotting and immunoprecipitation

Immunoblotting and immunoprecipitation were performed as previously described [17]. Briefly, microsomes were obtained from isolated tissues and cells. Samples were lysed with ice-cold lysis buffer with 10 mM Tris (pH 7.5), 150 mM NaCl, 1% Triton-X (Sigma-Aldrich), and 10% glycerol (Wako) containing a protease inhibitor cocktail and a phosphatase inhibitor cocktail (Nacalai tesque, Kyoto, Japan). For immunoprecipitation of HA-$Ca_V1.2$, lysates (125–250 μg/lane) containing HA-antibody (MBL, Nagoya, Japan) (3 μg) were incubated with Protein A-Sepharose (GE Healthcare Japan, Tokyo, Japan), and the immunoprecipitates were washed with the lysis buffer. For immunoblotting, samples were separated on SDS-PAGE using 4%–15% gradient gels. Primary and secondary antibodies against the following proteins were used: $Ca_V1.2$ (1:2,000, Alomone Labs, Jerusalem, Israel), c-Src (1:500, Santa Cruz Biotechnology, CA, USA), α-tubulin (1:3,000, Sigma-Aldrich), HA (1:5,000, MBL), phosphotyrosine (1:2,000, Abcam, Cambridge, UK), rabbit IgG (1:30,000), and mouse IgG (1:30,000) (Jackson ImmunoResearch Laboratories, West Grove, PA, USA). Anti-c-Src antibody was kindly provided by Dr. Toshikazu Takeshita (Shinshu University, Japan). Signal intensities of bands were quantified using the gel analysis program of the ImageJ software.

Proximity ligation assay and immunocytochemistry

A proximity ligation assay (PLA) was performed using the Duolink system (Sigma-Aldrich) in tsA201 cells cotransfected with cDNA for $Ca_V1.2$ channel subunits plus that for Myc-c-Src according to the manufacturer's instructions. Antibodies against $Ca_V1.2$ (1:200, Alomone) and Myc (1:2,000, MBL) were used as primary antibodies. Signals were visualized using Duolink In Situ PLA Probe Anti-Mouse PLUS, Duolink In Situ PLA Probe Anti-Rabbit MINUS, and Duolink In Situ Detection Reagents Orange (Sigma-Aldrich). Slides were mounted with Duolink In Situ Mounting Medium and DAPI (Sigma-Aldrich).

Z-stack images of the cells (pinhole size: 1 airy unit) were acquired using a laser scanning microscope TCS SP8 (Leica Microsystems), and the images were merged using the maximum projection program in the ImageJ software. For signal quantification, fluorescence images of PLA and nucleus signals were converted to binary images by the triangle and minimum methods, respectively, using the ImageJ software [24, 34]. In each merged image, the number of pixels with PLA positive signals was normalized to that of pixels with nucleus signals by using ImageJ software.

Statistics

All data are expressed as means ± SEM. Statistical significance was evaluated using the unpaired Student's t test. For multiple comparisons of data were performed using ANOVA followed by Dunnett's or Bonferroni's test. A $P < 0.05$ was considered statistically significant. All statistical analyses were performed using the SPSS software (SPSS Inc., Armonk, NY, USA).

Results

PDGF-induced VSMC migration by activating $Ca_V1.2$ Ca^{2+} channels through c-Src/Abl tyrosine kinases

A confluent monolayer of A7r5 cells was wounded and treated with vehicle or 10 ng/ml PDGF-BB for 48 h in a serum-free condition. Compared with the controls, PDGF-BB healed the wound significantly more intensely (Fig. 1a), indicating that PDGF-BB promoted migration and/or proliferation of VSMC [26] [36]. Moreover, a $Ca_V1.2$ channel inhibitor, nifedipine (Sigma-Aldrich), almost completely inhibited PDGF-induced wound healing in a concentration-dependent manner in a range of concentrations between 0.1 μM and 3 μM (Fig. 1b) as reported previously [4] [21]. PDGF activates various intracellular signaling proteins [6]. Thus, the molecule(s) that mediated the effect of PDGF were examined. SFK/Abl inhibitor, bosutinib, (Sigma-Aldrich) exhibited a much stronger inhibitory effect on the PDGF-induced wound healing than a PI3K inhibitor, wortmannin, (Cayman Chemical, Ann Arbor, MI, USA); an ERK inhibitor, SCH772984 (AdooQ Bioscience, Irvine, CA, USA); a p38 kinase inhibitor, VX-702 (Tokyo Chemical Industry); or a protein kinase C (PKC) inhibitor, Gö6983 (Wako) (Fig. 1c-g). Moreover, the effect of EHop-016, an inhibitor of an RFG, Rac1, was assessed; however, its strong cytotoxic effect precluded reliable analysis (data not shown). The fact that the proliferative PI3K and ERK played a minor role in the wound healing suggests that the result of this assay under the present condition mainly reflects the pro-migratory effect of PDGF. Thus, bosutinib inhibited PDGF-induced VSMC migration in a concentration-dependent manner (Fig. 1c). Of note, nifedipine and bosutinib did not show any additivity in inhibiting PDGF-induced migration (Fig. 1h), indicating that PDGF induced VSMC migration by activating $Ca_V1.2$ channels through SFK/Abl tyrosine kinases.

Direct evidence for PDGF-induced activation of $Ca_V1.2$ Ca^{2+} channels through SFKs

The extracellular application of 60 mM K^+ increased intracellular Ca^{2+} concentration much more strongly in PDGF-BB (10 ng/ml)-treated than that in control cells (Fig. 2a and b). This effect of PDGF was almost completely inhibited by bosutinib (2 μM) (Fig. 2b). However, PDGF-BB did not affect the expression level of $Ca_V1.2$ subunits nor c-Src (Fig. 2c and d), indicating that the effect of PDGF on $Ca_V1.2$ channels was posttranslational. In mock-transfected cells, PDGF significantly increased $Ca_V1.2$ channel Ba^{2+} currents in a range of the membrane potential between −30 and +30 mV (Fig. 2e). However, this effect of PDGF was not observed in cells transfected with CSK, a selective inhibitor of SFK (Fig. 2e). Therefore, PDGF increased the activity of $Ca_V1.2$ channels through SFK in VSMCs.

c-Src activates $Ca_V1.2$ Ca^{2+} channels with full-length $Ca_V1.2$ by enhancing the coupling efficiency between VSD and AG

Posttranslational modifications of $Ca_V1.2$ of VSMCs were assessed using immunoblotting (Fig. 3a). Full-length $Ca_V1.2$ ($Ca_V1.2$FL) and $Ca_V1.2$ with truncated C-terminus at 1763 a.a. ($Ca_V1.2\Delta1763$) were expressed in tsA201 cells and were immunoblotted as molecular markers of $Ca_V1.2$ without and with posttranslational modification, respectively. In synthetic A7r5 cells most of the expressed $Ca_V1.2$ was full-length (~240 KDa). In contrast, in contractile VSMCs in the rat aorta and cerebral artery and heart, both full-length and truncated $Ca_V1.2$ (~210 KDa) were expressed; these results are in agreement with those reported previously [1, 2, 5, 22] [23, 33]. These results suggest that PDGF induced the migration of A7r5 cells mainly by activating full-length $Ca_V1.2$.

Next, the effect of posttranslational modifications of $Ca_V1.2$ C-terminus on recombinant vascular $Ca_V1.2$ channels was examined. In this assay, tsA201 cells were transfected with cDNA for $Ca_V1.2$FL, $Ca_V1.2\Delta1763$, or $Ca_V1.2\Delta1763$ with clipped DCT together with cDNA for ancillary subunits β_{2a} and $\alpha_2\delta_1$ (Fig. 3b). The ratio of the ON gating charge of $Ca_V1.2$ channels elicited upon depolarization from −80 mV to E_{rev} and the amplitude of inward tail $Ca_V1.2$ channel Ba^{2+} currents upon repolarization to −70 mV (Fig.

3c, inset) was measured. This ratio reflected the coupling efficiency between VSD and AG. $Ca_V1.2\Delta1763$ channels showed a significantly higher ratio than $Ca_V1.2$FL channels, whereas $Ca_V1.2\Delta1763$ channels coexpressed with clipped DCT ($Ca_V1.2\Delta1763$ + DCT) exhibited a significantly smaller ratio than $Ca_V1.2\Delta1763$ channels (Fig. 3c). These results indicate that both "internal" DCT in $Ca_V1.2$FL and "clipped" DCT associated with $Ca_V1.2\Delta1763$ autoinhibited vascular $Ca_V1.2$ channel activity.

Further, effects of coexpression of c-Src on three types of $Ca_V1.2$ channels were assessed. Interestingly, c-Src significantly increased the coupling efficiency of $Ca_V1.2$FL channels, did not further increase that of $Ca_V1.2\Delta1763$ channels, and had no significant effect on $Ca_V1.2\Delta1763$ + DCT channels (Fig. 3d). c-Src significantly increased the Ca^{2+} current density of $Ca_V1.2$FL channels in a range of the membrane potentials between −20 and +30 mV (Fig. 3e). However, c-Src did not affect the voltage-dependency of steady-state activation or inactivation of $Ca_V1.2$FL channels (Fig. 3f, Table 1). Whether the failure of c-Src to activate $Ca_V1.2\Delta1763$ + DCT channels may be attributed to the overexpression of DCT compared with $Ca_V1.2\Delta1763$ in tsA201 cells and thus, very strong inhibition of the channel activity was examined. This may be because of the smaller nucleotide number and the consequent more efficient transcription of cDNA for DCT than that for $Ca_V1.2\Delta1763$. However, different molar ratios of cDNA of DCT and $Ca_V1.2\Delta1763$ failed to enable c-Src to activate $Ca_V1.2\Delta1763$ + DCT (Fig. 3g). In contrast, CK2α'β significantly activated $Ca_V1.2\Delta1763$ + DCT but not $Ca_V1.2$FL channels (Fig. 3h). These results strongly suggest that $Ca_V1.2$ channels with full-length $Ca_V1.2$ or truncated $Ca_V1.2$ associated with clipped DCT were both autoinhibited but were not functionally identical and subjected to differential regulations.

c-Src can bind to and phosphorylate full-length $Ca_V1.2$ channels

To elucidate the molecular mechanism underlying the selective effect of c-Src on $Ca_V1.2$FL, the phosphorylation of $Ca_V1.2$FL, $Ca_V1.2\Delta1763$, and $Ca_V1.2\Delta1763$ + DCT by c-Src was assessed. c-Src phosphorylated $Ca_V1.2$FL significantly more efficiently than $Ca_V1.2\Delta1763$ in the presence or absence of

DCT (Fig. 4a–c).

Next, the interaction between c-Src and three types of $Ca_V1.2$ channels was assessed by an *in situ* PLA. This assay visualizes the interaction of two proteins identified by two specific antibodies. This assay indicated that c-Src was significantly closer to $Ca_V1.2$FL channels than to $Ca_V1.2\Delta1763$ or $Ca_V1.2\Delta1763$ + DCT channels (Fig. 4d and e). Immunocytochemistry using the same antibodies used for PLA indicated that there was no statistical difference in expression levels of $Ca_V1.2$FL, $Ca_V1.2\Delta1763$, and $Ca_V1.2\Delta1763$ + DCT (data not shown). These results indicate that c-Src selectively activates $Ca_V1.2$FL channels because it can associate with and thus phosphorylate $Ca_V1.2$FL more efficiently than $Ca_V1.2\Delta1763$ irrespective of the presence or absence of DCT.

c-Src phosphorylation sites in full-length $Ca_V1.2$

Increased coupling efficiency of $Ca_V1.2$ channels through c-Src and effects of c-Src on $Ca_V1.2$ channels modulated by DCT suggest that c-Src may bind to and phosphorylate the C-terminus of $Ca_V1.2$. The C-terminus of $Ca_V1.2$ bears a total of 12 tyrosine residues (Fig. 5a). The C-terminus was first divided into PCT and DCT, and all tyrosine residues in PCT and DCT were mutated to phenylalanine residues (Fig. 5b). Mutations in PCT but not DCT completely inhibited the effect of c-Src on the coupling efficiency of $Ca_V1.2$FL channels (Fig. 5b). Next, PCT was divided into proximal PCT (PPCT) and distal PCT (DPCT), and all tyrosine residues in PPCT and DPCT were mutated to phenylalanine residues. The results of analysis of c-Src on these channels indicated that tyrosines in DPCT but not PPCT participated in the activation of $Ca_V1.2$ channels by c-Src (Fig. 5b). Finally, each tyrosine residue in DPCT was individually mutated to phenylalanine, which confirmed that c-Src activated $Ca_V1.2$FL channels by phosphorylating Tyr^{1709} and Tyr^{1758} in DPCT of $Ca_V1.2$FL channels (Fig. 5c).

Discussion

The present study confirmed for the first time that PDGF induces the migration of synthetic VSMCs by activating $Ca_V1.2$ channels with full-length $Ca_V1.2$ through SFK. Synthetic VSMCs represented by A7r5 cells expressed mainly full-length $Ca_V1.2$, but contractile VSMCs *in vivo* expressed both full-length and truncated $Ca_V1.2$. In assays using recombinant vascular $Ca_V1.2$ channels, c-Src could bind to and phosphorylate full-length $Ca_V1.2$ more efficiently in comparison to truncated $Ca_V1.2$ in the presence or absence of DCT. Moreover, c-Src activated $Ca_V1.2$ channels by phosphorylating Tyr^{1709} and Tyr^{1758} in the PCT of full-length $Ca_V1.2$. These results confirmed that phenotypic switching of VSMCs in atherosclerotic lesions may increase the ratio of full-length to truncated $Ca_V1.2$ channels and thereby facilitate PDGF-induced migration of VSMCs.

Among versatile signal transduction pathways activated by PDGFR, SFK, PI3K, MAPK, and RFG are implicated to play a role in cell migration [11]. However, we observed that SFK exerted much stronger pro-migratory effect on A7r5 cells than PI3K, MAPK, or PKC (Fig. 1). In addition, we observed that the PDGF-induced migration of A7r5 cells was strongly dependent on $Ca_V1.2$ channel activity. The effects of an SFK inhibitor, bosutinib, and a $Ca_V1.2$ channel inhibitor, nifedipine, did not exhibit additive effect, indicating that PDGF activated $Ca_V1.2$ channels through SFKs. In cell migration, intracellular Ca^{2+} plays a crucial role [15, 31]. In migrating cells, Ca_V1 channels evoke Ca^{2+} sparklets at the rear end. This channel activity increases intracellular Ca^{2+} concentration and causes actomyosin contraction to retract the trailing tail [18]. However, the mechanism through which SFK activate only $Ca_V1.2$ channels at the rear end of migrating VSMCs remains unclear. Recently, Kim et al. have reported that chemotactic signal (local epidermal growth factor receptor stimulation) at the front edge of human umbilical endothelial cells activated the whole-cell Ca_V1 channels through PI3K, whereas PKC more strongly inhibited Ca_V1 channels closer to the receptors at the front edge [18]. Because in our case, inhibitors of PI3K and PKC were not

effective, different mechanism(s) may underlie the localized activation of $Ca_V1.2$ channels in VSMCs.

In a heterologous expression system, c-Src activated $Ca_V1.2$FL channels by enhancing the coupling efficiency between VSD and AG. This indicated that c-Src inhibited the autoinhibitory effect of DCT in $Ca_V1.2$FL. This effect of c-Src was mediated by the phosphorylation of Tyr^{1709} and Tyr^{1758} in PCT. Different from PKA, c-Src did not shift the activation curve of $Ca_V1.2$ channels in the hyperpolarizing direction. This is probably because of different amino acid residues phosphorylated by these kinases. It is also possible that different modes of action of PKA and c-Src may account for the difference: PKA activates $Ca_V1.2$ channels composed of truncated $Ca_V1.2$ and clipped DCT whereas c-Src activates $Ca_V1.2$FL channels. Tyr^{1709} and Tyr^{1758} in PCT are novel regulatory sites identified in this study. Kang's previous study on the human vascular $Ca_V1.2$-b has indicated that c-Src first phosphorylates Tyr^{2134} of $Ca_V1.2$, recognizes this phosphotyrosine with its own SH2 domain, and then phosphorylates Tyr^{1837} of $Ca_V1.2$ to activate $Ca_V1.2$ channels [16]. Of these two sites, Tyr^{2134} corresponds to Tyr^{2136} in our B8 clone, whereas Tyr^{1837} is replaced with serine in our B8 clone. The reason for the discrepancy between our and Kang's results remains unclear, but this could be attributed to various possibilities. First, Kang's analysis was restricted to DCT; thus, the effects of phosphorylation of tyrosine residues in PCT might have been overlooked. Second, a slight and insignificant decrease in the effect of c-Src on $Ca_V1.2$FL DCT-YF compared with that on $Ca_V1.2$FL (Fig. 5b) may indicate the phosphorylation of Tyr^{2136} (corresponding to Tyr^{2134} in their $Ca_V1.2$-b). Finally, we coexpressed $\alpha_2\delta_1$ subunits with $Ca_V1.2$ and β_2 subunits, such a different subunit composition of $Ca_V1.2$ channels may have affected the results.

c-Src significantly activated $Ca_V1.2$FL channels but not $Ca_V1.2\Delta1763$ or $Ca_V1.2\Delta1763$ + DCT channels (Fig. 3d). As mentioned above, it was likely that c-Src activated $Ca_V1.2$FL channels by inhibiting the autoinhibitory effect of DCT. It is, therefore, plausible that c-Src might not further activate un-autoinhibited $Ca_V1.2\Delta1763$ channels. However, it was puzzling why c-Src did not activate autoinhibited $Ca_V1.2\Delta1763$ + DCT channels. We first considered a possibility that in our construct, DCT may be

overexpressed in comparison with $Ca_V1.2\Delta1763$ in tsA201 cells and thereby caused very strong inhibition on the channel activity. However, this was not the case because a wide range of DCT-to-$Ca_V1.2\Delta1763$ cDNA molar ratios did not enable c-Src to activate $Ca_V1.2\Delta1763$ + DCT channels (Fig. 3g). Therefore, we suggest that $Ca_V1.2$ channels became unresponsive to c-Src irrespective of the degree of autoinhibition once its $Ca_V1.2$ C-terminus was clipped. Interestingly, CK2 efficiently activated $Ca_V1.2\Delta1763$ + DCT channels (Fig. 3h), but it failed to activate $Ca_V1.2$FL channels. We also observed the same results regarding the differential regulation of cardiac $Ca_V1.2$ channels by c-Src and CK2 [17]. These results strongly suggest that $Ca_V1.2$ channels with full-length $Ca_V1.2$ and those with truncated $Ca_V1.2$ associated with clipped DCT were both autoinhibited but were not functionally identical and subjected to differential regulations.

Our results indicate that c-Src can more efficiently bind to and phosphorylate $Ca_V1.2$FL than $Ca_V1.2\Delta1763$ or $Ca_V1.2\Delta1763$ + DCT channels (Fig. 4). It was proposed that c-Src binds to the proline-rich domain (PRD) in DCT via its SH3 domain (Fig. 6) [10] [16]. Thus, c-Src would not be able to bind to $Ca_V1.2\Delta1763$ because it is devoid of PRD. It is also suggested that cleaved DCT associates with PCT via the same PRD [10]. Thus, we propose that c-Src cannot activate $Ca_V1.2\Delta1763$ + DCT channels because the binding of c-Src to PRD in clipped DCT is precluded by the putative PRD acceptor site(s) (PAS) in PCT (Fig. 6). Namely, $Ca_V1.2\Delta1763$, DCT, and c-Src may not form a ternary complex. In $Ca_V1.2$FL channels, DCT may not noncovalently bind to internal PCT via the PRD; thus, c-Src may be able to bind to PRD. Notably, c-Src weakly but unmistakably interacted with and phosphorylated $Ca_V1.2\Delta1763$ + DCT channels (Fig. 4). This interaction may arise from the interaction of c-Src with another PRD in the intracellular loop between domains II and III of $Ca_V1.2$ [7]. However, our study did not delineate the functional significance of this phosphorylation.

To summarize, our findings demonstrate that PDGF induces the migration of synthetic VSMCs by activating $Ca_V1.2$ channels with full-length $Ca_V1.2$ through SFK. Moreover, in contrast to contractile VSMCs, synthetic VSMCs express full-length $Ca_V1.2$ more strongly than truncated $Ca_V1.2$. It is possible

that contractile VSMCs are less migratory than synthetic VSMCs at least in part because the substantial fraction of $Ca_V1.2$ in contractile VSMCs is converted into the truncated form. Clipped DCT enters the nucleus and serves as a transcriptional factor [12], suppressing the transcription of $Ca_V1.2$ gene in cardiac myocytes and VSMCs [2, 27]. Thus, when VSMCs undergo a phenotypic switching in atherosclerotic lesions, the inhibition of posttranslational modification of the C-terminus of $Ca_V1.2$ may increase the ratio of full-length $Ca_V1.2$ to truncated $Ca_V1.2$ and enhance the transcription of $Ca_V1.2$ *per se*. We posit that such phenotypic switching may coordinately facilitate the pro-migratory effects of PDGF on VSMCs.

Figure legends

Fig. 1. PDGF induces vascular smooth muscle cell migration dependent on $Ca_V1.2$ channels and Src/Abl tyrosine kinases

(a) PDGF-induced VSMC migration. Representative images of wound healing assay of A7r5 cells with vehicle (control) or 10 ng/ml PDGF-BB for 48 h in a serum-free condition (left-hand panel). Scale bar, 200 μm. Dashed yellow lines indicate original wound area. Wound healing ratio of A7r5 cells with vehicle (n = 12) or 10 ng/ml PDGF-BB (n = 7) for 48 h (right-hand panel). *$P < 0.05$ *versus* control. (b–g) effects of pharmacological inhibitors on the PDGF-induced migration of A7r5 cells. A7r5 cells were treated with PDGF-BB in the presence of vehicle, nifedipine (b, n = 6–9), bosutinib (c, n = 6–10), wortmannin (d, n = 6–14), SCH772984 (e, n = 10–14), VX-702 (f, n = 6–7), or Gö6983 (g, n = 7–10). *$P < 0.05$ *versus* each PDGF-treated A7r5 cells in the presence of vehicle. (h) less-than-additive effects of nifedipine and bosutinib on the PDGF-induced migration of A7r5 cells. Representative images (left-hand panel) and wound healing ratio (right-hand panel) of PDGF-treated A7r5 cells in the presence of vehicle (n = 9), 0.3 μM nifedipine alone (n = 8), 0.1 μM bosutinib alone (n = 11), or 0.3 μM nifedipine plus 0.1 μM bosutinib (n = 13). *$P < 0.05$ *versus* PDGF-treated A7r5 cells in the presence of vehicle.

Fig. 2. PDGF activates $Ca_V1.2$ channels through c-Src family kinases

(a) representative traces of 60 mM K^+-induced $[Ca^{2+}]_i$ elevation in A7r5 cells pretreated with vehicle or with PDGF for 24 h in a serum-free condition. (b) effects of bosutinib (2 μM) on 60 mM K^+-induced $[Ca^{2+}]_i$ elevation in control and PDGF-treated A7r5 cells. The number of observed cells is indicated in the graph. *$P < 0.05$ *versus* each control cells. (c and d) representative immunoblots of $Ca_V1.2$ (c) and c-Src (d) from three independent experiments in control and PDGF-treated A7r5 cells (each left-hand panel). The whole-cell lysates ($Ca_V1.2$; 50 μg/lane, c-Src; 20 μg/lane, tubulin; 20 μg/lane) were immunoblotted with

antibodies against $Ca_V1.2\alpha_{1c}$, c-Src, and tubulin. The summary of the data normalized to tubulin; n = 3 independent blots (each right-hand panel). *P < 0.05 *versus* control. (e) representative traces of Ba^{2+} currents of $Ca_V1.2$ channels in control and PDGF-treated A7r5 cells expressing mock (upper left-hand panel) or CSK (upper right-hand panel). Voltage protocol (inset). Effect of PDGF on peak current density–voltage relationships of $Ca_V1.2$ channels with Ba^{2+} as a charge carrier in control and PDGF-treated A7r5 cells expressing mock or CSK (lower panels); n = 8–19. *P < 0.05 *versus* each control.

Fig, 3. Activation of recombinant full-length $Ca_V1.2$ channels by c-Src

(a) a representative immunoblot of $Ca_V1.2$ from three independent experiments. Lysates (50 μg/lane) from indicated samples were immunoblotted with antibody against $Ca_V1.2$. This antibody binds to the intracellular linker between domains II and II of $Ca_V1.2$. Lysates from tsA201 cells transfected with mock, full-length $Ca_V1.2$ ($Ca_V1.2$FL), and $Ca_V1.2\Delta1763$ channels were used as negative or positive controls. (b) schematic illustration of $Ca_V1.2$FL, $Ca_v1.2\Delta1763$, and $Ca_v1.2\Delta1763$ + DCT channels. (c) coupling efficiencies (nA/pC) of $Ca_V1.2$FL, $Ca_v1.2\Delta1763$, and $Ca_v1.2\Delta1763$ + DCT channels in tsA201 cells; n = 6–8. Representative traces of gating currents and Ba^{2+} tail currents of $Ca_v1.2$ Ca^{2+} channels, and voltage protocol (insets). *P < 0.05 *versus* $Ca_V1.2$FL channels, $^{\#}P$ < 0.05 *versus* $Ca_v1.2\Delta1763$ channels. (d) effect of Myc-c-Src overexpression on coupling efficiencies of $Ca_V1.2$FL, $Ca_v1.2\Delta1763$, and $Ca_v1.2\Delta1763$ + DCT channels in tsA201 cells; n = 7–10. *P < 0.05 *versus* each mock. (e) effect of Myc-c-Src overexpression on peak current density–voltage relationships of $Ca_V1.2$FL Ca^{2+} currents in tsA201 cells expressing mock (n = 7) or Myc-c-Src (n = 5). *P < 0.05 *versus* mock. (f) effect of Myc-c-Src overexpression on steady-state activation and inactivation of $Ca_V1.2$FL Ca^{2+} currents in tsA201 cells expressing mock or Myc-c-Src; n = 7–8. (g) the effect of Myc-c-Src on the coupling efficiency of $Ca_V1.2\Delta1763$ + DCT channels with different molar ratios of DCT to $Ca_V1.2\Delta1763$; n = 5–11 cells in each ratio. There was no statistically significant difference between mock and c-Src groups at any molar ratios. (h) effect of CK2α'β overexpression on

coupling efficiencies of $Ca_V1.2$FL and $Ca_v1.2\Delta1763$ + DCT channels in tsA201 cells; n = 6–9. *$P < 0.05$ *versus* each mock.

Fig. 4. Interaction between $Ca_V1.2$ Ca^{2+} channels and c-Src

(a–c) c-Src more potently phosphorylated $Ca_V1.2$FL than $Ca_v1.2\Delta1763$ with or without DCT. HA- $Ca_V1.2$ channels and Myc-c-Src were expressed in tsA201 cells as indicated. HA-$Ca_V1.2$ subunits were immunoprecipitated (IP) with antibody against HA from lysates and analyzed by immunoblotting (IB) with antibodies against phosphotyrosine (pTyr, a) and HA (b). a and b are representative immunoblots from four different experiments. NS, nonspecific band. (c) quantification of phosphorylated $Ca_V1.2$ ($Ca_V1.2$-pTyr)/total $Ca_V1.2$. Data were normalized to $Ca_V1.2$FL-pTyr/total $Ca_V1.2$FL. *$P < 0.05$ *versus* $Ca_V1.2$FL + c-Src group. There was no statistically significant difference between $Ca_V1.2\Delta1763$ + c-Src and $Ca_v1.2\Delta1763$ + DCT + c-Src groups. (d) representative images showing the association of $Ca_V1.2$FL, $Ca_V1.2\Delta1763$, or $Ca_v1.2\Delta1763$ + DCT channels with c-Src as detected by PLA assay. $Ca_V1.2$ channels and Myc-c-Src were expressed in tsA201 cells as indicated. Protein–protein association between $Ca_V1.2$ channels and c-Src was visualized as orange signals. Nuclei were stained with DAPI (blue). Scale bars, 25 μm. (e) quantification of association of $Ca_V1.2$FL, $Ca_V1.2\Delta1763$, or $Ca_V1.2\Delta1763$ + DCT channels with c-Src; 40 images from four coverslips in each group. Data were normalized to the ratio of $Ca_V1.2$FL + c-Src. *$P < 0.01$ *versus* $Ca_V1.2\alpha_{1C}$FL + c-Src.

Fig. 5. Requirement for phosphorylation of Tyr^{1709} and Tyr^{1758} for c-Src-mediated activation of $Ca_V1.2$ channels

(a) schematic representation of all tyrosine residues (indicated as Y) in the C-terminus of $Ca_V1.2$ ($Ca_V1.2$CT). PCT (proximal C-terminus); DCT (distal C-terminus); PPCT (proximal proximal C-terminus); DPCT (distal proximal C-terminus). (b) the coupling efficiency of $Ca_V1.2$FL channels in which all tyrosine

residues were mutated to phenylalanine within the indicated regions of $Ca_V1.2$CT. (c) the coupling efficiency of $Ca_V1.2$FL channels in which tyrosine residues were individually mutated to phenylalanine; n = 5–15 cells. *$P < 0.05$ *versus* each mock.

Fig. 6. Proposed mechanism underlying the selective effect of c-Src on full-length $Ca_V1.2$

In $Ca_V1.2$FL, c-Src can bind to the proline-rich domain (PRD, 1945–1970 aa) in DCT through its SH3 domain (SH3) and thereby can phosphorylate Y1709 and Y1758 in PCT (left-hand panel). c-Src cannot bind to $Ca_V1.2\Delta1763$ because it is devoid of PRD (middle panel). Clipped DCT is associated with truncated PCT via interactions between DCRD (2070–2082 aa) and PCRD (1664–1674 aa) and between PRD and a putative PRD acceptor site (PAS) in PCT (right-hand panel). Because PRD in clipped DCT is already occupied by PAS in this case, c-Src can no longer bind to $Ca_V1.2$ and phosphorylate Y1709 or Y1758. Y, tyrosine; S, serine; SH2, SH2 domain; KN, kinase N-lobe; and KC, kinase C-lobe.

Compliance with Ethical Standards

Disclosure of potential conflicts of interest

This study was supported by Grant-in-Aid for Scientific Research (C) (grant number 16K08546) to T.K. from the Ministry of Education, Culture, Sports, Science and Technology, Japan and a grant to M.Y. from Shinshu Public Utility Foundation for Promotion of Medical Sciences.

Research involving Animals

All animals used in the present study received humane care in compliance with the Guide for the Care and Use of Laboratory Animals published by the US National Institutes of Health. All experimental procedures were performed in accordance with the Guidelines for Animal Experimentation of Shinshu University and approved by the Committee for Animal Experimentation (Approval number 260017).

References

1. Bannister JP, Adebiyi A, Zhao G, Narayanan D, Thomas CM, Feng JY, and Jaggar JH. Smooth muscle cell alpha2delta-1 subunits are essential for vasoregulation by CaV1.2 channels. *Circulation research* 105: 948-955, 2009.

2. Bannister JP, Leo MD, Narayanan D, Jangsangthong W, Nair A, Evanson KW, Pachuau J, Gabrick KS, Boop FA, and Jaggar JH. The voltage-dependent L-type Ca2+ (CaV1.2) channel C-terminus fragment is a bi-modal vasodilator. *The Journal of physiology* 591: 2987-2998, 2013.

3. Catterall WA, Wisedchaisri G, and Zheng N. The chemical basis for electrical signaling. *Nature chemical biology* 13: 455-463, 2017.

4. Corsini A, Bonfatti M, Quarato P, Accomazzo MR, Raiteri M, Sartani A, Testa R, Nicosia S, Paoletti R, and Fumagalli R. Effect of the new calcium antagonist lercanidipine and its enantiomers on the migration and proliferation of arterial myocytes. *Journal of cardiovascular pharmacology* 28: 687-694, 1996.

5. De Jongh KS, Murphy BJ, Colvin AA, Hell JW, Takahashi M, and Catterall WA. Specific phosphorylation of a site in the full-length form of the alpha 1 subunit of the cardiac L-type calcium channel by adenosine 3',5'-cyclic monophosphate-dependent protein kinase. *Biochemistry* 35: 10392-10402, 1996.

6. Demoulin JB, and Essaghir A. PDGF receptor signaling networks in normal and cancer cells. *Cytokine & growth factor reviews* 25: 273-283, 2014.

7. Dubuis E, Rockliffe N, Hussain M, Boyett M, Wray D, and Gawler D. Evidence for multiple Src binding sites on the alpha1c L-type Ca2+ channel and their roles in activity regulation. *Cardiovascular research* 69: 391-401, 2006.

8. Fu Y, Westenbroek RE, Yu FH, Clark JP, 3rd, Marshall MR, Scheuer T, and Catterall WA. Deletion

of the distal C terminus of CaV1.2 channels leads to loss of beta-adrenergic regulation and heart failure in vivo. *The Journal of biological chemistry* 286: 12617-12626, 2011.

9. Fuller MD, Emrick MA, Sadilek M, Scheuer T, and Catterall WA. Molecular mechanism of calcium channel regulation in the fight-or-flight response. *Science signaling* 3: ra70, 2010.

10. Gerhardstein BL, Gao T, Bunemann M, Puri TS, Adair A, Ma H, and Hosey MM. Proteolytic processing of the C terminus of the alpha(1C) subunit of L-type calcium channels and the role of a proline-rich domain in membrane tethering of proteolytic fragments. *The Journal of biological chemistry* 275: 8556-8563, 2000.

11. Gerthoffer WT. Mechanisms of vascular smooth muscle cell migration. *Circulation research* 100: 607-621, 2007.

12. Gomez-Ospina N, Tsuruta F, Barreto-Chang O, Hu L, and Dolmetsch R. The C terminus of the L-type voltage-gated calcium channel Ca(V)1.2 encodes a transcription factor. *Cell* 127: 591-606, 2006.

13. Hell JW, Westenbroek RE, Breeze LJ, Wang KK, Chavkin C, and Catterall WA. N-methyl-D-aspartate receptor-induced proteolytic conversion of postsynaptic class C L-type calcium channels in hippocampal neurons. *Proceedings of the National Academy of Sciences of the United States of America* 93: 3362-3367, 1996.

14. Hulme JT, Yarov-Yarovoy V, Lin TW, Scheuer T, and Catterall WA. Autoinhibitory control of the CaV1.2 channel by its proteolytically processed distal C-terminal domain. *The Journal of physiology* 576: 87-102, 2006.

15. Iamshanova O, Fiorio Pla A, and Prevarskaya N. Molecular mechanisms of tumour invasion: regulation by calcium signals. *The Journal of physiology* 595: 3063-3075, 2017.

16. Kang M, Ross GR, and Akbarali HI. COOH-terminal association of human smooth muscle calcium channel Ca(v)1.2b with Src kinase protein binding domains: effect of nitrotyrosylation.

American journal of physiology Cell physiology 293: C1983-1990, 2007.

17. Kashihara T, Nakada T, Kojima K, Takeshita T, and Yamada M. Angiotensin II activates CaV 1.2 Ca2+ channels through beta-arrestin2 and casein kinase 2 in mouse immature cardiomyocytes. *The Journal of physiology* 595: 4207-4225, 2017.

18. Kim JM, Lee M, Kim N, and Heo WD. Optogenetic toolkit reveals the role of Ca2+ sparklets in coordinated cell migration. *Proceedings of the National Academy of Sciences of the United States of America* 113: 5952-5957, 2016.

19. Kumar S, Collins W, Egan A, Yadava A, Garraud O, Blackman MJ, Guevara Patino JA, Diggs C, and Kaslow DC. Immunogenicity and efficacy in aotus monkeys of four recombinant Plasmodium falciparum vaccines in multiple adjuvant formulations based on the 19-kilodalton C terminus of merozoite surface protein 1. *Infection and immunity* 68: 2215-2223, 2000.

20. Libby P. Inflammation in atherosclerosis. *Arteriosclerosis, thrombosis, and vascular biology* 32: 2045-2051, 2012.

21. Patel MK, Clunn GF, Lymn JS, Austin O, and Hughes AD. Effect of serum withdrawal on the contribution of L-type calcium channels (CaV1.2) to intracellular Ca2+ responses and chemotaxis in cultured human vascular smooth muscle cells. *British journal of pharmacology* 145: 811-817, 2005.

22. Pesic A, Madden JA, Pesic M, and Rusch NJ. High blood pressure upregulates arterial L-type Ca2+ channels: is membrane depolarization the signal? *Circulation research* 94: e97-104, 2004.

23. Pratt PF, Bonnet S, Ludwig LM, Bonnet P, and Rusch NJ. Upregulation of L-type Ca2+ channels in mesenteric and skeletal arteries of SHR. *Hypertension* 40: 214-219, 2002.

24. Prewitt JM, and Mendelsohn ML. The analysis of cell images. *Annals of the New York Academy of Sciences* 128: 1035-1053, 1966.

25. Raines EW. PDGF and cardiovascular disease. *Cytokine & growth factor reviews* 15: 237-254,

2004.

26. Saxty BA, Yadollahi-Farsani M, Kefalas P, Paul S, and MacDermot J. Inhibition of chemotaxis in A7r5 rat smooth muscle cells by a novel panel of inhibitors. *British journal of pharmacology* 125: 152-158, 1998.

27. Schroder E, Byse M, and Satin J. L-type calcium channel C terminus autoregulates transcription. *Circulation research* 104: 1373-1381, 2009.

28. Sheng X, Nakada T, Kobayashi M, Kashihara T, Shibazaki T, Horiuchi-Hirose M, Gomi S, Hirose M, Aoyama T, and Yamada M. Two mechanistically distinct effects of dihydropyridine nifedipine on CaV1.2 L-type Ca(2)(+) channels revealed by Timothy syndrome mutation. *European journal of pharmacology* 685: 15-23, 2012.

29. Sonkusare S, Palade PT, Marsh JD, Telemaque S, Pesic A, and Rusch NJ. Vascular calcium channels and high blood pressure: pathophysiology and therapeutic implications. *Vascular pharmacology* 44: 131-142, 2006.

30. Tang ZZ, Hong X, Wang J, and Soong TW. Signature combinatorial splicing profiles of rat cardiac- and smooth-muscle Cav1.2 channels with distinct biophysical properties. *Cell calcium* 41: 417-428, 2007.

31. Wei C, Wang X, Zheng M, and Cheng H. Calcium gradients underlying cell migration. *Current opinion in cell biology* 24: 254-261, 2012.

32. Wei X, Neely A, Lacerda AE, Olcese R, Stefani E, Perez-Reyes E, and Birnbaumer L. Modification of Ca2+ channel activity by deletions at the carboxyl terminus of the cardiac alpha 1 subunit. *The Journal of biological chemistry* 269: 1635-1640, 1994.

33. Xue JH, Zhang LF, Ma J, and Xie MJ. Differential regulation of L-type Ca2+ channels in cerebral and mesenteric arteries after simulated microgravity in rats and its intervention by standing. *American journal of physiology Heart and circulatory physiology* 293: H691-701, 2007.

34. Zack GW, Rogers WE, and Latt SA. Automatic measurement of sister chromatid exchange frequency. *The journal of histochemistry and cytochemistry : official journal of the Histochemistry Society* 25: 741-753, 1977.

35. Zamponi GW, Striessnig J, Koschak A, and Dolphin AC. The Physiology, Pathology, and Pharmacology of Voltage-Gated Calcium Channels and Their Future Therapeutic Potential. *Pharmacological reviews* 67: 821-870, 2015.

36. Zhu Y, Bujo H, Yamazaki H, Hirayama S, Kanaki T, Takahashi K, Shibasaki M, Schneider WJ, and Saito Y. Enhanced expression of the LDL receptor family member LR11 increases migration of smooth muscle cells in vitro. *Circulation* 105: 1830-1836, 2002.

Table 1: Kinetic parameters of Cav1.2 Ca^{2+} channels

	Control	n	c-Src	n
Steady-state activation				
G_{max} (pS/pF)	511 ± 58	7	858 ± 93*	8
$E_{0.5\_Act}$ (mV)	-3.9 ± 2.2	7	-8.5 ± 0.8	8
k_{Act} (mV)	7.2 ± 0.5	7	6.5 ± 0.4	8
E_{rev} (mV)	60.2 ± 4.1	7	70.6 ± 2.1	8
Steady-state inactivation				
f_0	0.23 ± 0.03	7	0.22 ± 0.03	8
$E_{0.5\_Inact}$ (mV)	-17.57 ± 0.69	7	-17.19 ± 0.48	8
k_{Inact} (mV)	9.81 ± 1.37	7	8.69 ± 0.84	8

*G_{max}: maximum conductance density; $E_{0.5\_Act}$: half-maximum activation potential; k_{Act}: slope factor of activation; E_{rev}: apparent reversal potential; f_0, an offset at depolarized potential; $E_{0.5\_Inact}$: half-maximum inactivation potential; k_{Inact}: slope factor of inactivation. *$P < 0.05$ vs. Control*

Figure 1

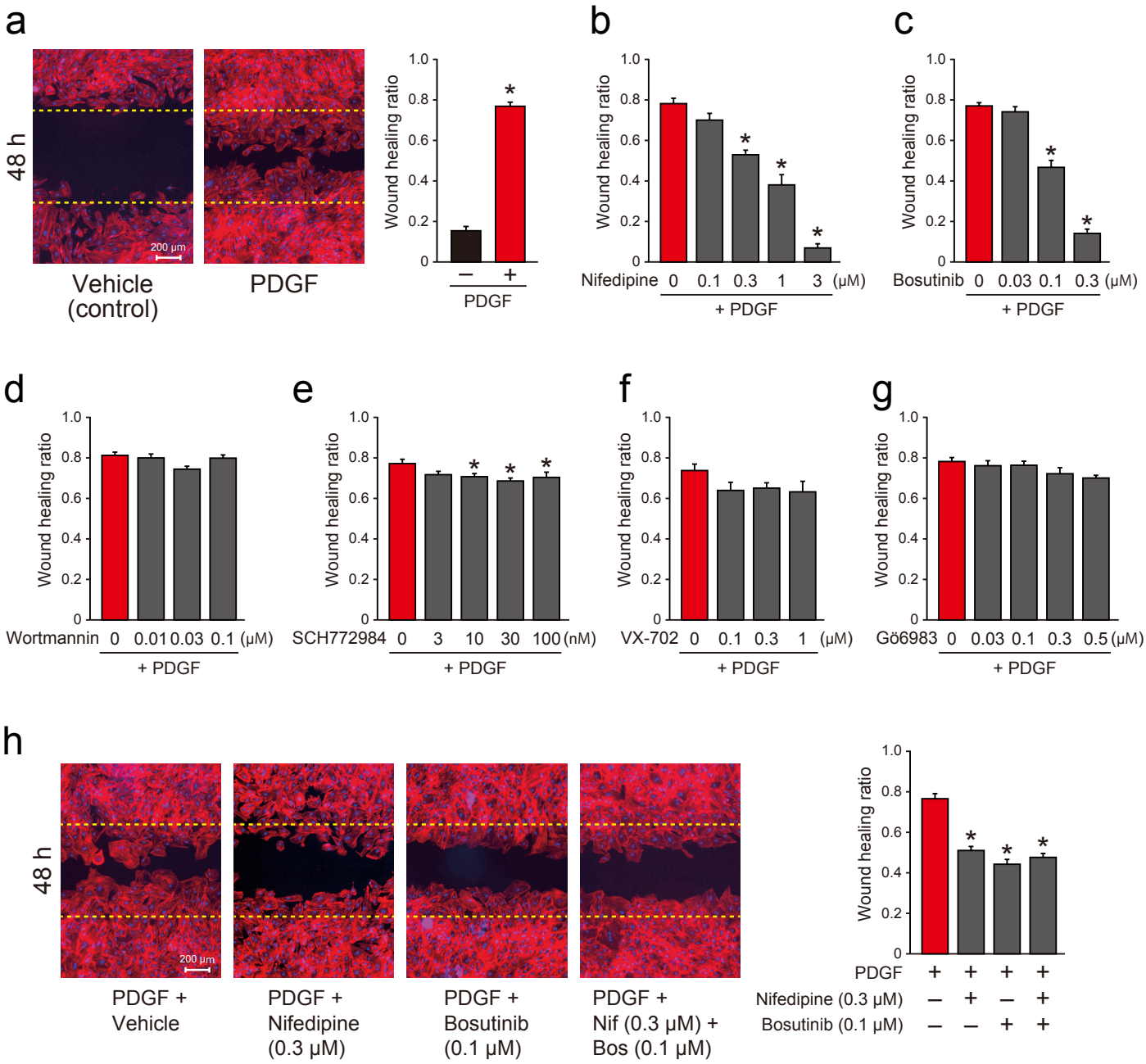
a
48 h
200 μm
Vehicle (control)
PDGF
Wound healing ratio
1.0
0.8
0.6
0.4
0.2
0
*
–
+
PDGF
b
Wound healing ratio
Nifedipine 0 0.1 0.3 1 3 (μM)
+ PDGF
c
Wound healing ratio
Bosutinib 0 0.03 0.1 0.3 (μM)
+ PDGF
d
Wound healing ratio
Wortmannin 0 0.01 0.03 0.1 (μM)
+ PDGF
e
Wound healing ratio
SCH772984 0 3 10 30 100 (nM)
+ PDGF
f
Wound healing ratio
VX-702 0 0.1 0.3 1 (μM)
+ PDGF
g
Wound healing ratio
Gö6983 0 0.03 0.1 0.3 0.5 (μM)
+ PDGF
h
48 h
200 μm
PDGF + Vehicle
PDGF + Nifedipine (0.3 μM)
PDGF + Bosutinib (0.1 μM)
PDGF + Nif (0.3 μM) + Bos (0.1 μM)
Wound healing ratio
PDGF + + + +
Nifedipine (0.3 μM) – + – +
Bosutinib (0.1 μM) – – + +

Figure 2

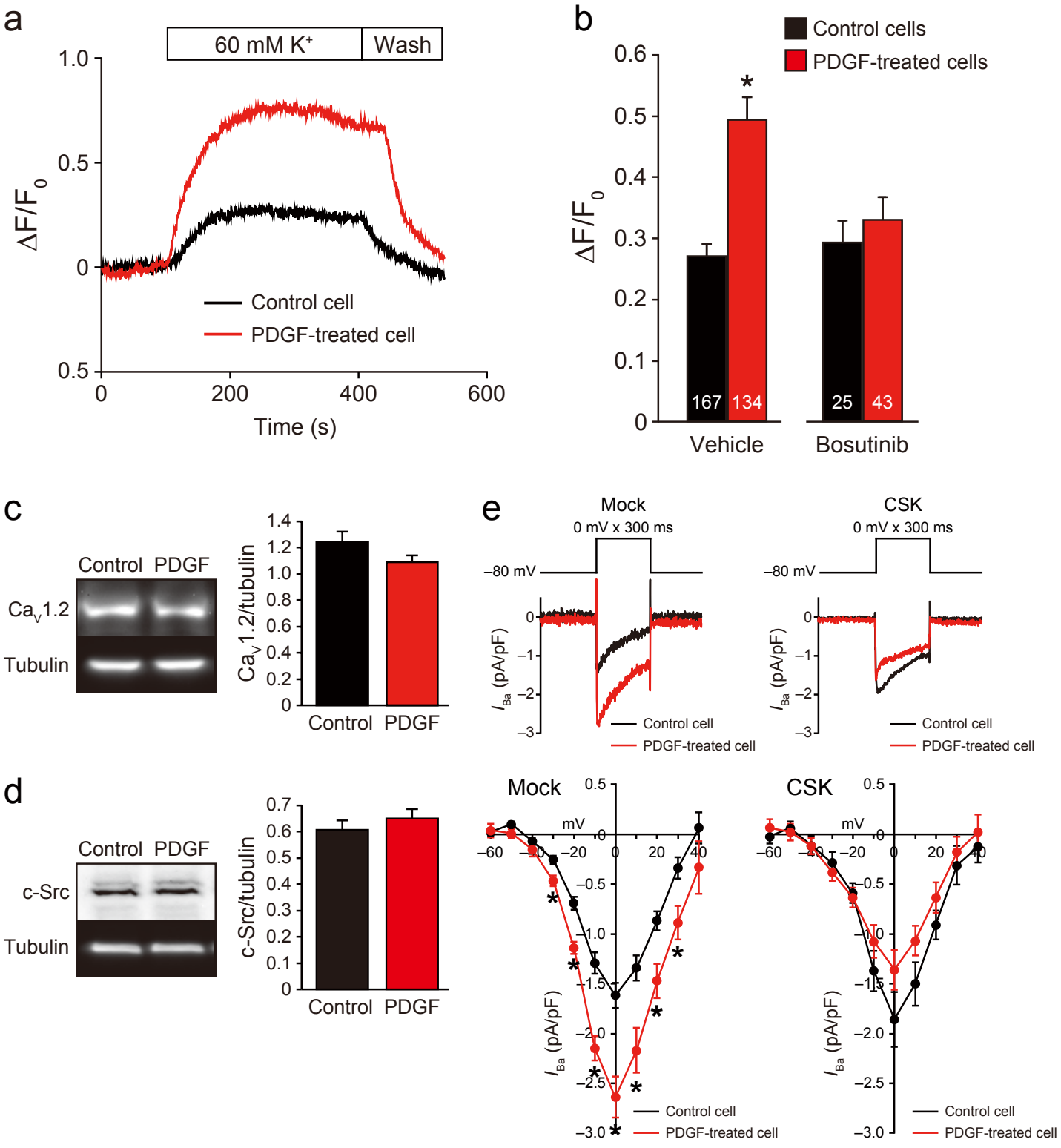
a
60 mM K+
Wash
ΔF/F0
Time (s)
Control cell
PDGF-treated cell
b
Control cells
PDGF-treated cells
ΔF/F0
167
134
25
43
Vehicle
Bosutinib
c
Control PDGF
CaV1.2
Tubulin
CaV1.2/tubulin
Control PDGF
d
Control PDGF
c-Src
Tubulin
c-Src/tubulin
Control PDGF
e
Mock
CSK
0 mV x 300 ms
−80 mV
IBa (pA/pF)
Control cell
PDGF-treated cell
mV

Figure 3

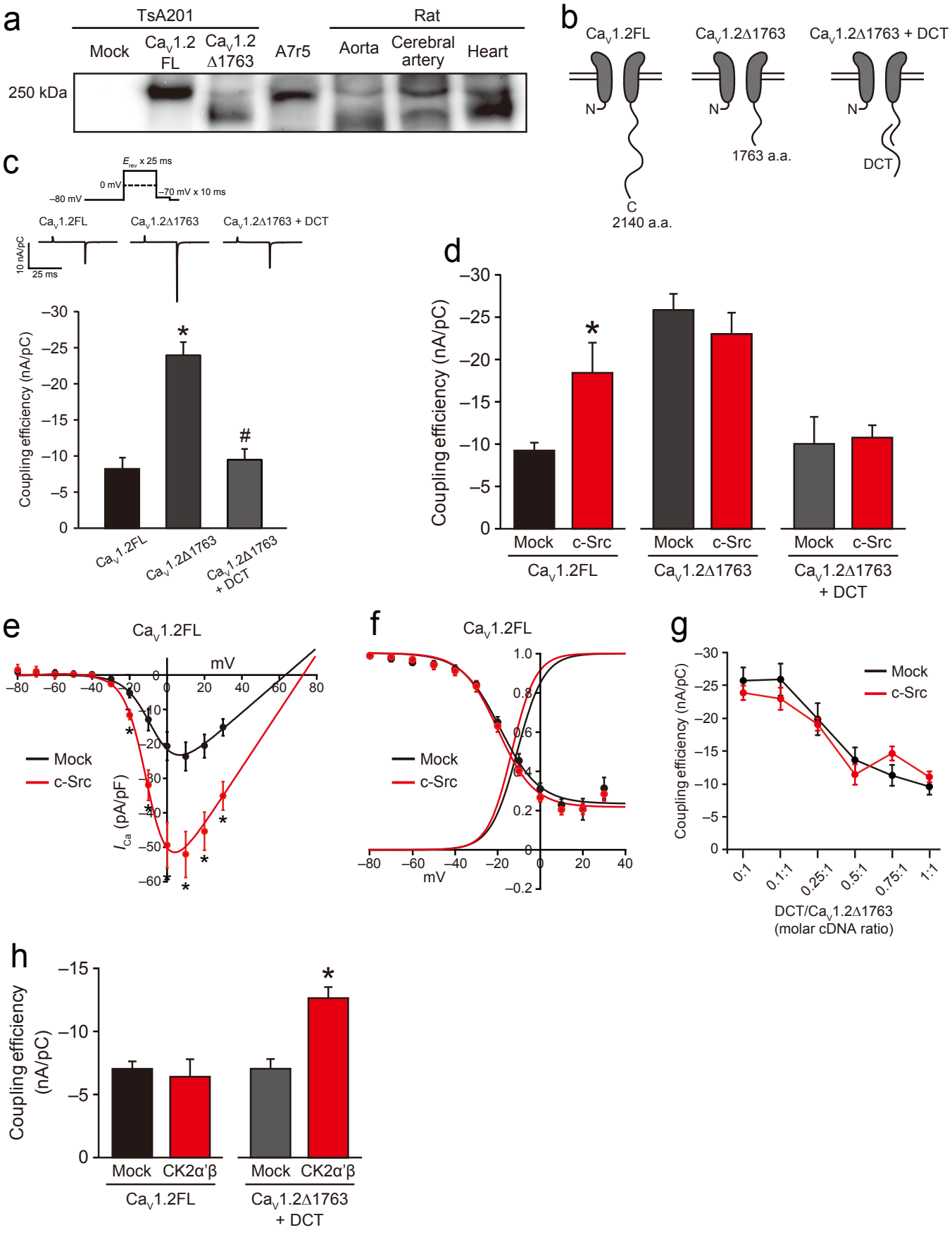
a
TsA201
Rat
Mock
CaV1.2 FL
CaV1.2 Δ1763
A7r5
Aorta
Cerebral artery
Heart
250 kDa
b
CaV1.2FL
CaV1.2Δ1763
CaV1.2Δ1763 + DCT
N
C
2140 a.a.
1763 a.a.
DCT
c
Erev x 25 ms
0 mV
–80 mV
–70 mV x 10 ms
10 nA/pC
25 ms
Coupling efficiency (nA/pC)
d
Mock
c-Src
e
CaV1.2FL
mV
ICa (pA/pF)
f
g
DCT/CaV1.2Δ1763
(molar cDNA ratio)
0:1
0.1:1
0.25:1
0.5:1
0.75:1
1:1
h
CK2α'β
CaV1.2Δ1763 + DCT

Figure 4

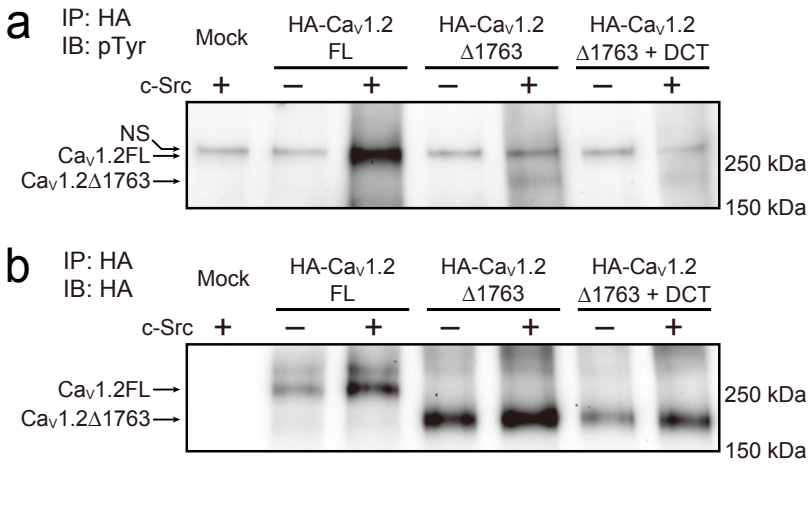
a
IP: HA
IB: pTyr
Mock
HA-CaV1.2 FL
HA-CaV1.2 Δ1763
HA-CaV1.2 Δ1763 + DCT
c-Src + – + – + – +
NS
CaV1.2FL
CaV1.2Δ1763
250 kDa
150 kDa
b
IP: HA
IB: HA
Mock
HA-CaV1.2 FL
HA-CaV1.2 Δ1763
HA-CaV1.2 Δ1763 + DCT
c-Src + – + – + – +
CaV1.2FL
CaV1.2Δ1763
250 kDa
150 kDa

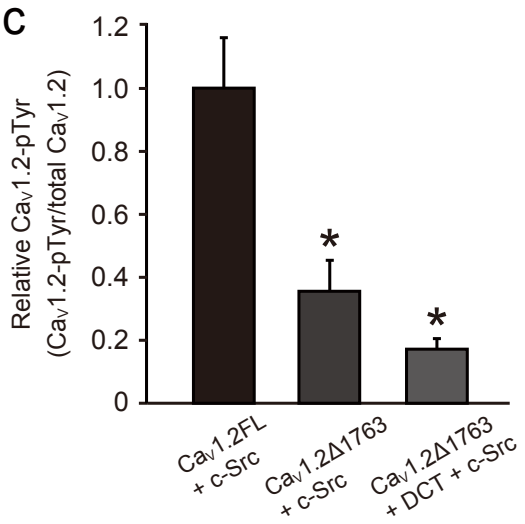
c
Relative CaV1.2-pTyr (CaV1.2-pTyr/total CaV1.2)
1.2
1.0
0.8
0.6
0.4
0.2
0
*
*
CaV1.2FL + c-Src
CaV1.2Δ1763 + c-Src
CaV1.2Δ1763 + DCT + c-Src

d

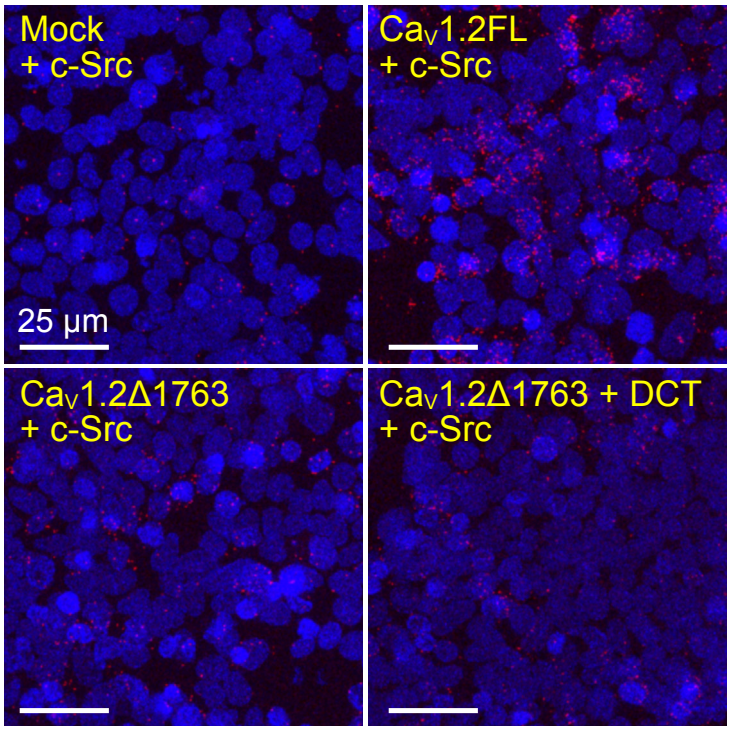
Mock + c-Src
CaV1.2FL + c-Src
25 µm
CaV1.2Δ1763 + c-Src
CaV1.2Δ1763 + DCT + c-Src

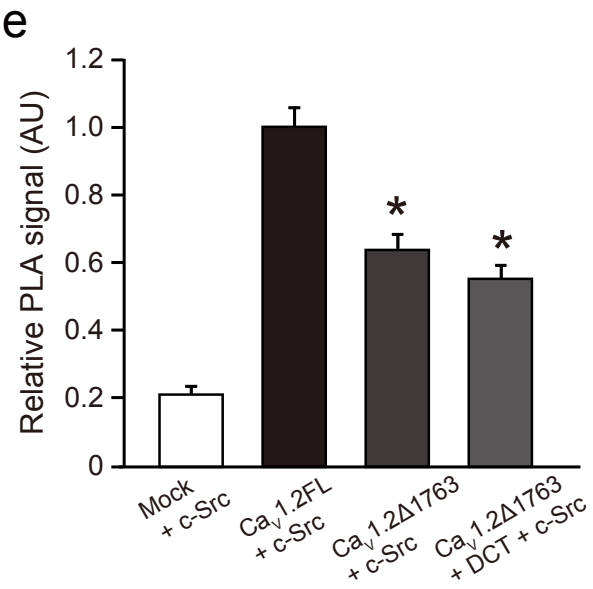
e
Relative PLA signal (AU)
1.2
1.0
0.8
0.6
0.4
0.2
0
*
*
Mock + c-Src
CaV1.2FL + c-Src
CaV1.2Δ1763 + c-Src
CaV1.2Δ1763 + DCT + c-Src

Figure 5

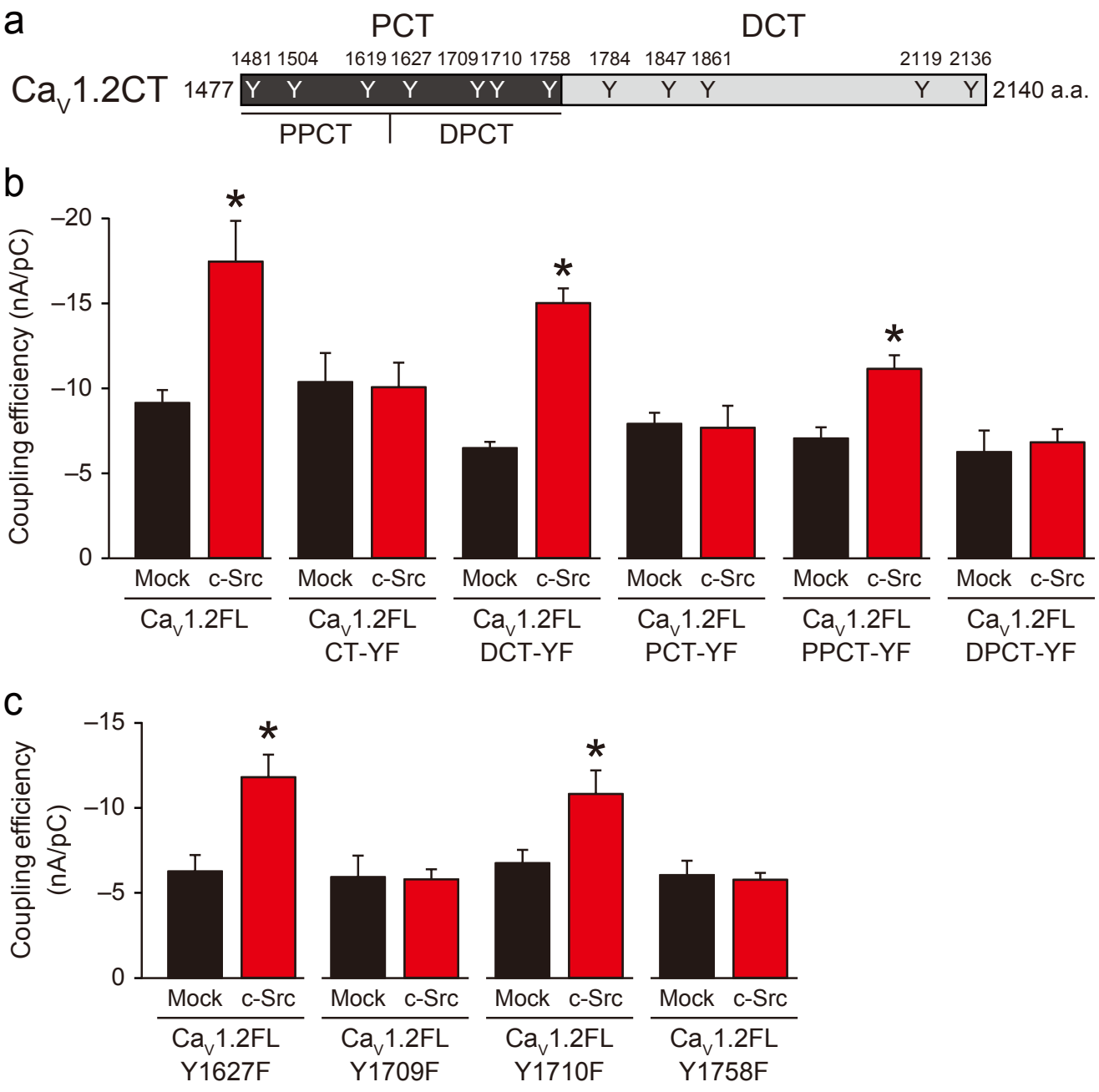
a
PCT
DCT
1481 1504
1619 1627 1709 1710 1758
1784
1847 1861
2119 2136
Ca$_V$1.2CT
1477
Y Y Y Y Y Y Y
Y Y Y
Y Y
2140 a.a.
PPCT
DPCT
b
Coupling efficiency (nA/pC)
–20
–15
–10
–5
0
*
Mock
c-Src
Ca$_V$1.2FL
Ca$_V$1.2FL CT-YF
Ca$_V$1.2FL DCT-YF
Ca$_V$1.2FL PCT-YF
Ca$_V$1.2FL PPCT-YF
Ca$_V$1.2FL DPCT-YF
c
Coupling efficiency (nA/pC)
–15
–10
–5
0
Ca$_V$1.2FL Y1627F
Ca$_V$1.2FL Y1709F
Ca$_V$1.2FL Y1710F
Ca$_V$1.2FL Y1758F

Figure 6

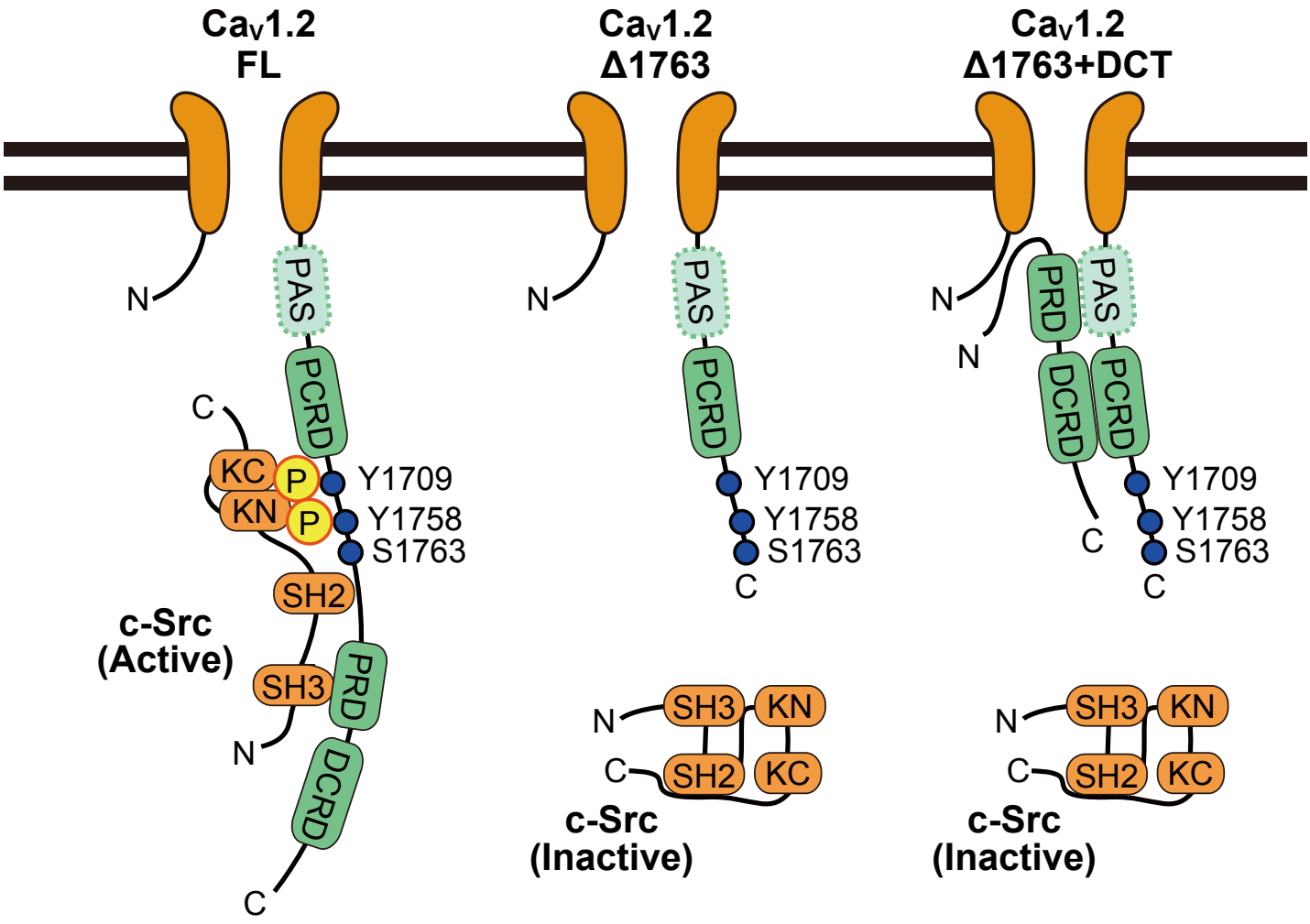
Cav1.2
FL
Cav1.2
Δ1763
Cav1.2
Δ1763+DCT
N
PAS
PCRD
C
KC
KN
P
P
Y1709
Y1758
S1763
SH2
SH3
PRD
DCRD
c-Src
(Active)
PRD
DCRD
SH3
KN
SH2
KC
c-Src
(Inactive)